ACS APPLIED MATERIALS & INTERFACES

Research Article

www.acsami.org

One-Pot Synthesis of Mesoporous TiO_2 Microspheres and Its Application for High-Efficiency Dye-Sensitized Solar Cells

Zhao-Qian Li,[†] Ya-Ping Que,[†] Li-E Mo,[†] Wang-Chao Chen, Yong Ding,[†] Yan-Mei Ma,[†] Ling Jiang,[†] Lin-Hua Hu,*[,†] and Song-Yuan Dai*[,†,‡]

[†]Key Laboratory of Novel Thin-Film Solar Cells, Institute of Applied Technology, Hefei Institutes of Physical Science, Chinese Academy of Sciences, Hefei, Anhui 230031, PR China

[‡]Beijing Key Laboratory of Novel Thin-Film Solar Cells, North China Electric Power University, Beijing 102206, PR China

ABSTRACT: TiO_2 microspheres are of great interest for a great deal of applications, especially in the solar cell field. Because of their unique microstructure and light-scattering effect, TiO_2 microsphere-based solar cells often exhibit superior photovoltaic performance. Hence, exploring new suitable TiO_2 microspheres for high-efficiency solar cells is essential. In this work, we demonstrate a facile one-pot solvothermal approach for synthesis of TiO_2 microspheres using acetone as solvent. The as-prepared TiO_2 microspheres are composed of densely interconnected nanocrystals and possess a high specific surface area up to 138.47 $m^2\ g^{-1}$. As the photoanode, the TiO_2 microsphere-based DSSC gives higher dye loading and light adsorption ability as well as longer electron lifetime, resulting in higher short-circuit current value and superior power conversion efficiency (PCE) compared with Dyesol 18 nm TiO_2 nanoparticle paste. Finally, the TiO_2 microsphere-based DSSC were optimized by adding a TiO_2 nanocrystal underlayer and $TiCl_4$ post-treatment, giving a high PCE of 10.32%.

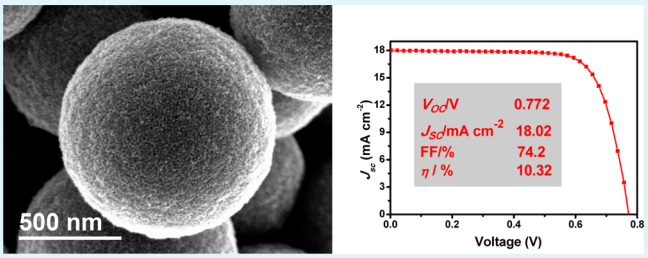

KEYWORDS: *mesoporous materials, TiO_2, microspheres, dye-sensitized solar cell, acetone*

1. INTRODUCTION

As an important inorganic semiconductor, anatase titanium dioxide (TiO_2) has been widely investigated in a range of applications, such as photocatalysis,[1,2] hydrogen generation,[3,4] Li-ion batteries,[5,6] and utilized as the photoanode for dye-sensitized solar cells (DSSC).[7−11] As an important part of DSSC, generally, a photoanode with high BET surface area and dye loading capacity, fast electron transport, and a pronounced light-scattering effect for better light absorption is indispensable. Thus, optimizing the photoanode structure to boost its performance on DSSC is necessary. To date, various strategies have been developed, e.g., $TiCl_4$ post-treatment,[12−14] optimizing the size of TiO_2 nanocrystals,[15,16] constructing 1D membranes,[17,18] or using submicro-/microsized spheres,[19−22] hollow,[23,24] and hierarchical-structured[25,26] TiO_2 as photoanode. Among these strategies, DSSCs employing TiO_2 microspheres as electrode have demonstrated superior performance because of its well-interconnected nanocrystallinity, high special surface area, and strong scattering ability.[13,27,28] For example, Cheng et al., employing TiO_2 beads as photoanode, fabricated DSSC and compared it with Degussa P25. The bead-based DSSC shows longer diffusion lengths and extended electron life, resulting in power conversion efficiency (PCE) as high as 10.6%.[13] Grätzel et al. reported a mesoporous TiO_2-bead-based DSSC using YD2-o-C8 dye and cobalt-based redox electrolyte. Compared with TiO_2-nanoparticle-based photoanode, electrolyte diffusion through these films can be greatly improved because of the large interstitial pores between the TiO_2 beads, and consequently, an efficiency of 11.4% is achieved.[27] However, synthesis of these TiO_2 beads often needs template or complicated process. Thus, considering the practical value for DSSCs, the TiO_2 microspheres should be further investigated, and at the same time, developing new morphological microspheres or a new facial synthesis method and applying it to DSSC is still a pressing need.

In this work, mesoporous TiO_2 microspheres (MS) with densely interconnected nanocrystallinity and high surface area were synthesized by a one-pot solvothermal method using acetone as the solvent. Under heating treatment, the reaction system can produce water by the aldol condensation of acetone in the presence of metal complexes, and then the resulting water acts as oxygen for the formation of TiO_2.[4,29] Subsequently, the as-obtained TiO_2 MS were used as photoanode to fabricate DSSC; the TiO_2-MS-based DSSC exhibits much higher dye loading ability, stronger light absorption, and longer electron lifetime compared with the commercial Dyesol 18 nm TiO_2 nanoparticle paste, resulting in a high short-circuit current and remarkable performance with regard to PCE.

Received: March 12, 2015
Accepted: May 6, 2015
Published: May 6, 2015

DOI: 10.1021/acsami.5b02195
ACS Appl. Mater. Interfaces 2015, 7, 10928−10934

2. RESULTS AND DISCUSSION

TiO_2 MS were synthesized according to a modified procedure.[4] Figure 1a shows scanning electron microscopy (SEM) images

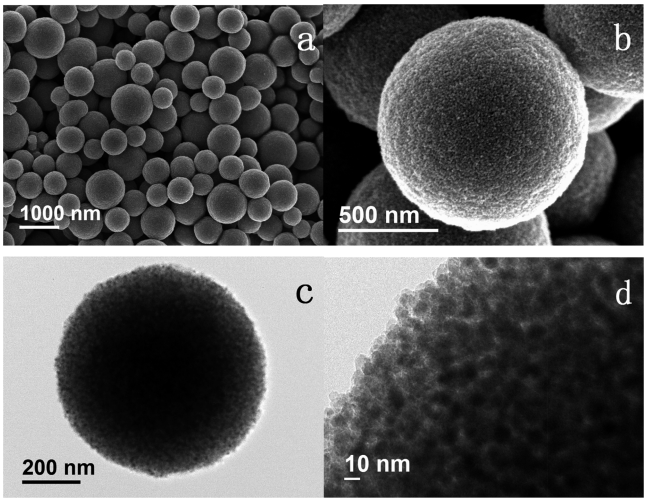

Figure 1. (a and b) SEM and (c and d) TEM images of the TiO_2 MS synthesized at 200 °C for 12 h.

of TiO_2 spheres with a diameter range of 550−1050 nm directly obtained by solvothermal treatment at 200 °C for 12 h. These spheres all have a beautiful shape and are composed of densely interconnected TiO_2 crystals (Figure 1b). The transmission electron microscopy (TEM) images show that the spheres have lighter contrast along the edge compared to the center, which reveals that these spheres have a porous nanostructure (Figure 1c). Also, from The HRTEM image (Figure 1d), one can clearly see that the microspheres have interconnected mesopores and are composed of nanocrystallites with a width of ∼12 nm.

As working electrodes for DSSCs, TiO_2 films should be annealed at 510 °C for 30 min; therefore, it is necessary to examine the crystalline condition of the TiO_2 MS after annealing. Therefore, the XRD patterns of the TiO_2 MS before and after annealing were conducted. As shown in Figure 2a, the diffraction peak of the TiO_2 MS after sintering corresponding to (101) planes (most intense peak) became smaller and broader than that of the TiO_2 MS before sintering treatment. The average crystal size increases from 11.86 to 13.97 nm as calculated by the Scherrer equation. As a comparison, a standard nanocrystalline TiO_2 sample composed of roughly 18 nm particles (Dyesol-18 nm paste, denoted as DSL-18) was also characterized (Figure 2a). After sintering under the same conditions as TiO_2 MS, the crystal size of the commercial Dyesol sample is 20.17 nm as calculated by the Scherrer equation according to the XRD pattern.

Specific surface areas (Brunauer−Emmett−Teller, BET) and pore size distribution (Barret−Joyner−Halenda, BJH) of the TiO_2 MS and DSL-18 after sintering were analyzed by nitrogen adsorption−desorption. As shown in Figure 2b,c, the commercial DSL-18 nanocrystalline TiO_2 sample has a wide pore size distribution and the average pore diameter is 29.9 nm. The specific surface area for DSL-18, calculated by the BET method, is 75.9 $m^2\ g^{-1}$. Compared with the commercial DSL-18 sample, the as-prepared TiO_2 MS has a narrower pore size distribution, and the average value is 9.2 nm, indicating that the sample has very uniform mesopores. The specific surface area for TiO_2 MS is as high as 138.47 $m^2\ g^{-1}$, which is much higher than that of DSL-18. Such high BET surface area could facilitate the dye-loading capacity and might endow the MS-based DSSCs with higher current density.

To investigate the light-scattering effect, dye-loading capacity, and DSSC properties, the TiO_2 MS-based film with a thickness of 7 μm was prepared via screen-printing method (Figure 3a). As a comparison, DSL-18 film was also controlled at the same thickness (Figure 3b). Here, the prepared TiO_2 MS are expected to provide dual function in DSSCs: higher light-scattering effect, by the submicro-/microsize of the spheres, and dye-loading capacity, by the much larger BET surface area. To confirm the light-scattering effect of the TiO_2 MS-based photoanode film, the diffuse reflectance of the TiO_2 MS- and DSL-18-based films was measured using an integrating sphere. Figure 3c shows that TiO_2 MS film has higher diffuse reflection capacities in the entire wavelength range from 300 to 800 nm than DSL-18 film. Notably, as the wavelength increased from 400 to 800 nm, the DSL-18 film shows a rapid decrease in diffuse reflection property, whereas the TiO_2 MS film still keeps a higher light diffuse reflection capacity in these visible and near-infrared regions, suggesting that light scattering for the TiO_2 MS is significantly enhanced with respect to DSL-18 because of the sphere size that is comparable to the wavelength of visible light.

For DSSCs, the amount of dye loading on the photoanode film significantly affects its current density. Therefore, the saturation adsorption of C101 dye was measured by UV−vis spectroscopy after desorbing the dye. As shown in Figure 3d, the absorbance intensity of dye desorbed from TiO_2 MS is higher than that from DSL-18, suggesting that for the same film

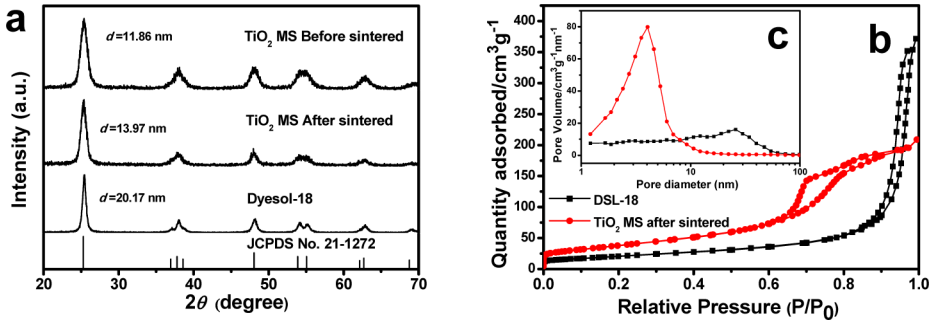

Figure 2. (a) XRD patterns of the TiO_2 MS before and after sintering, and Deysol-18 nm (DSL-18) paste sintered at 450 °C for 30 min. (b) Nitrogen adsorption/desorption isotherms of the TiO_2 MS and DSL-18 after sintering. (c) Corresponding Barret−Joyner−Halenda (BJH) pore size distribution plots.

DOI: 10.1021/acsami.5b02195
ACS Appl. Mater. Interfaces 2015, 7, 10928−10934

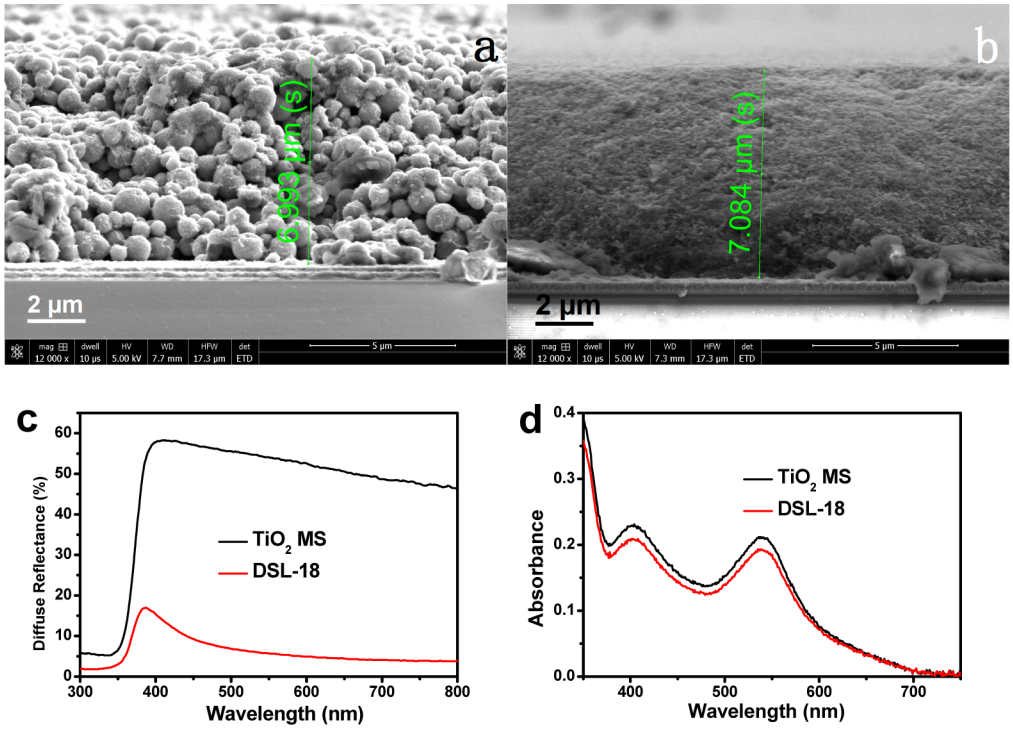

Figure 3. Cross-sectional SEM images of (a) TiO_2 MS- and (b) DSL-18-based films. (c) Diffuse reflectance spectra and (d) dye desorbed from anode filMS-based on TiO_2 MS and DSL-18.

Table 1. Comparison of the Photovoltaic Properties Measured under 1 Sun Illumination and Dye Adsorption Capacities for TiO_2 MS- and DSL-18-Based DSSCs

cell	thickness (μm)	dye loading (10^{-8} mol cm^{-2})	J_{sc} (mA cm^{-2})	V_{oc} (V)	FF (%)	η (%)
TiO_2 MS	7	9.69	13.89	0.761	73.77	7.80
DSL-18	7	8.82	11.88	0.759	74.81	6.76

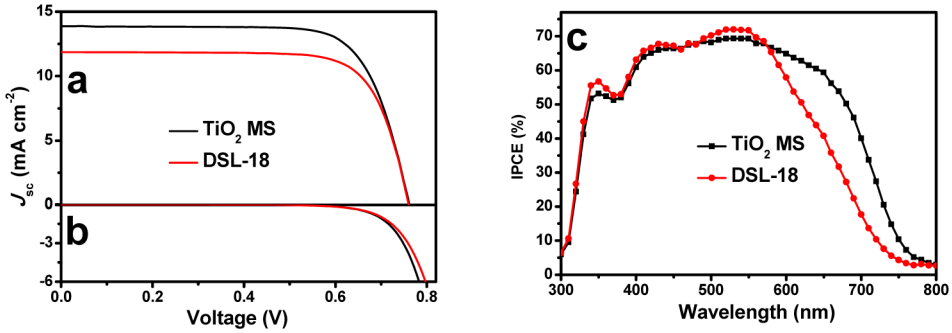

Figure 4. Current-density−voltage (J−V) characteristics (a) under illumination and (b) in the dark. (c) Incident photon-to-electron conversion efficiencies (IPCE) of TiO_2 MS- and DSL-18-based DSSCs.

thickness TiO_2 MS-based film has higher dye-loading capacity (Table 1).

To explore the photovoltaic properties of the TiO_2 microspheres, we fabricated complete solar cells. The resulting C101-sensitized DSSCs based on TiO_2 MS and DSL-18 were characterized by measuring the J−V behavior with an active area of 5 × 5 mm^2 under 1 sun illumination and in the dark and the IPCE properties. Figure 4a shows the short-circuit current density (J_{sc}) versus open circuit voltage (V_{oc}) curves of TiO_2 MS and DSL-18-based DSSCs. The detailed photovoltaic parameters are summarized in Table 1. Compared with DSL-18, the TiO_2 MS-based DSSC has the same V_{oc}, a bit lower FF, whereas it demonstrates a much higher J_{sc} (13.89 mA cm^{-2}). As a result, a higher η value of 7.8% was obtained, which was 15.4% greater than that of DSL-18 (6.76%). The higher photocurrent of TiO_2 MS-based DSSC might lie in two reasons: (1) the higher BET surface area, providing sufficient dye-loading to the surface of TiO_2 for more light harvesting and (2) better light-utilizing efficiency, owing to the superior light-scattering effect of microspheres. Indeed, the fact that TiO_2 MS-based DSSC has much better light-utilizing efficiency can be evidenced by the IPCE characterization. As shown in Figure 4c, in the short wavelength region from 300 to 580 nm, DSL-18 has a IPCE value similar to that of TiO_2 MS-based DSSC. However, in the long wavelength region (580−800 nm), the TiO_2 MS-based DSSC possesses an IPCE value higher than

DOI: 10.1021/acsami.5b02195
ACS Appl. Mater. Interfaces 2015, 7, 10928−10934

that of DSL-18-based DSSC. The higher IPCE value of the TiO_2 MS-based DSSC should be attributed to the enhanced light-scattering capacity of the microspheres, which promote the light capture of dye in this region. The result is also in good agreement with diffuse reflection results analyzed above.

The electron recombination rate plays an important role for the electron collection, transport and, eventually, the current density, the PCE of DSSC. Dark current of the DSSC induced by the reduction of I_3^- ions by the electron on the conduction band could reflect the charge recombination condition.[25,30] Here, we conducted dark current potential scans to estimate the electron recombination of the TiO_2 MS- and DSL-18-based DSSCs (Figure 4b). Compared with DSL-18-based DSSC, the dark current onset of the TiO_2 MS-based DSSC shifts to a lower potential and produces a higher dark current at the same potential above 0.6 V, suggesting that the TiO_2 MS-based DSSC has a higher electron recombination rate than DSL-18. The higher recombination rate can be ascribed to the densely interconnected smaller crystal sizes (14 nm) of the TiO_2 MS compared to those of DSL-18 (20 nm). The smaller crystal size endows the TiO_2 MS with a higher surface area, and nevertheless, it will produce more traps and electron acceptors for charge recombination than DSL-18 when it is applied to DSSC.[15,31,32]

To better understand the dynamics of electron transport and recombination, electrochemical impedance spectroscopy (EIS) of TiO_2 MS- and DSL-18-based DSSCs is measured at −0.73 V forward bias in the dark (Figure 5); the fitting data results are

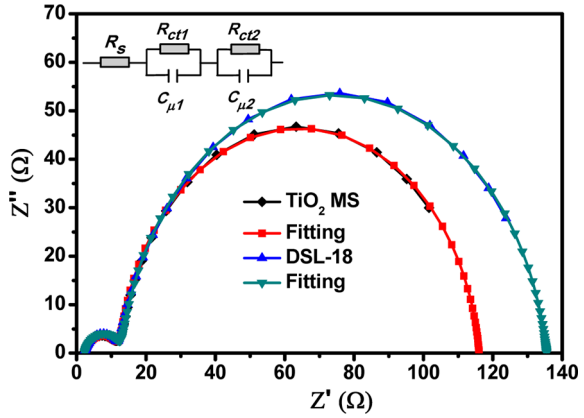

Figure 5. Nyquist plots of TiO_2 MS- and DSL-18-based DSSCs measured at −0.73 V forward bias in dark.

Table 2. Electron Transfer and Recombination Resistance (R_{ct}) and Chemical Capacitance (C_μ) of the TiO_2 MS- and DSL-18-Based DSSCs

cell	R_{ct} (Ω)	C_μ (μF)	$\tau_{n(EIS)}$ (ms)
TiO_2 MS	103.6	661	68.5
DSL-18	122.6	446	54.7

summarized in Table 2. Compared with DSL-18, the TiO_2 MS-based DSSC has a lower charge-transfer and recombination resistance (R_{ct}), suggesting that it has a higher recombination rate; this observation is in agreement with the results of dark current measurement mentioned above. However, despite the lower R_{ct}, the TiO_2 MS has a larger C_μ value, which is a constant-phase element resulting from the capacitor components in the cell. On the basis of the fitting data R_{ct} and C_μ, the electron lifetime ($\tau_{n(EIS)} = R_{ct} \times C_\mu$) values[30] are calculated to be 68.5 and 54.7 ms for TiO_2 MS- and DSL-18-based DSSCs, respectively. Clearly, the TiO_2 MS-based DSSC show a longer electron lifetime. The reason might be that the good interconnectivity of the TiO_2 crystals within the microspheres facilitates electron transport owing to less grain boundaries. This longer electron lifetime should be a direct reason for the higher current density and PCE in the TiO_2 MS-based DSSC under light illumination.

In addition to the EIS measurement, the evolution of the electron lifetime (τ_n) and the electron transport time (τ_d) as a function of short-circuit current (J_{sc}) were also determined using the rate constants derived from photovoltage and photocurrent decay measurements (Figure 6). Compared with DSL-18-based DSSC, the electron transport time is longer in the TiO_2 MS film in the entire range of J_{sc} (Figure 6a). The electron transport time is related to the electron recombination rate in a DSSC. In this work, as analyzed above, the crystal size of the as-obtained TiO_2 MS is smaller than that of DSL-18, and the TiO_2 MS-based DSSC has a smaller recombination resistance. Therefore, the recombination rate is higher in the MS-based DSSC than in the DSL-18-based DSSC, consequently resulting in a longer electron transport time. Besides, in the DSL-18-based electrode, there will be many voids produced by sintering the TiO_2 paste during the film preparation process that would result in less interconnections between particles. Although the TiO_2 crystals are densely interconnected within the microspheres, there will be more crystal boundaries in the MS-based photoanode, which would likewise lead to more electron recombination. Thus, the electron transport time in the TiO_2 MS-based DSSC is longer than that in the DSL-18-based DSSC.

Figure 6b shows the plot of the electron lifetime as a function of J_{sc}. In the entire range of J_{sc}, the TiO_2 MS-based DSSC all exhibit a superior electron lifetime compared with that of the DSL-18 DSSCs. The result is consistent with the above EIS analyses. Apart from this, interestingly, at a higher J_{sc}, the τ_n of TiO_2 MS has a much larger value than that of DSL-18, namely, the higher the light intensity, the larger the τ_n value difference. The electron lifetime is related to the recombination events occurring during cell operation and is defined as the time that electrons can survive before recombination. So, in other words, if the cell could generate more electrons under the same light illumination, then there will be more opportunity for the generated electrons to survive in the DSSC, resulting in a longer electron lifetime. In this research, because of the superior light-scattering ability, BET surface area, and dye loading capacity, the TiO_2 MS-based DSSC can generate much more electrons than DSL-18 at higher light intensity. Additionally, the large interstitial voids formed between the TiO_2 spheres could facilitate the electrolyte diffusion at higher current density. Thus, at higher J_{sc}, the TiO_2 MS-based DSSC shows much a longer electron lifetime than DSL-18. Coincidentally, Grätzel's group have likewise reported a similar phenomenon induced by submicro/microspheres.[27] They studied the diffusion of cobalt-based electrolytes in a TiO_2 bead-based photoanode and compared it with a DSL-18-based photoanode; the results revealed that the DSSC composed of the bead photoanode show less diffusion limitation. In the submicrosized bead-based DSSC, the generated electrons can

DOI: 10.1021/acsami.5b02195
ACS Appl. Mater. Interfaces 2015, 7, 10928−10934

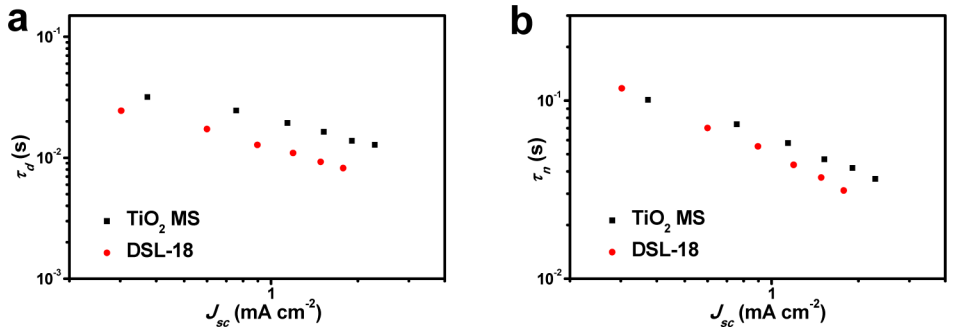

Figure 6. (a) Electron transport time and (b) electron lifetime as a function of short-current density for TiO_2 MS-and DSL-18-based DSSCs.

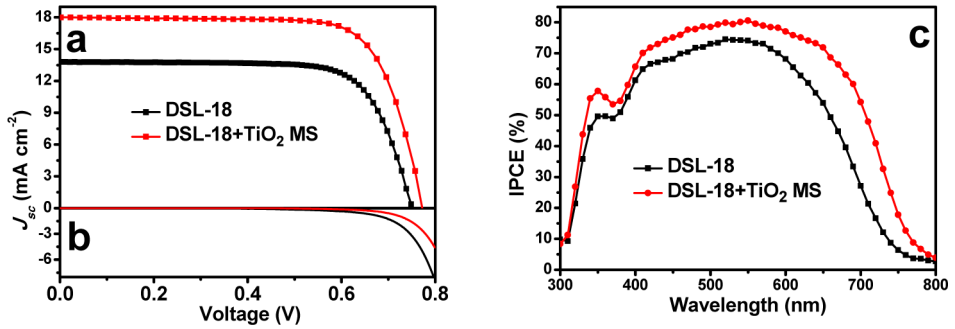

Figure 7. $J-V$ characteristics (a) under the illumination and (b) in the dark. (c) Incident photon-to-electron conversion efficiencies (IPCE) of the optimized photoanode-film-based DSSCs.

efficiently transport, viz, less pronounced "current spikes" at higher light intensity.

Owing to the large submicro/micrometer size of the as-obtained TiO_2 MS (550−1050 nm), some light might be backscattered at the FTO−TiO_2 interface; therefore, this part of light cannot be utilized by the dye to generate electrons. It is reported that a small-sized TiO_2 nanoparticle (NP) underlayer can reduce this loss.[27,33] First, the NP underlayer provides considerable BET surface area for dye loading, and its high transparency would allow the transmittance of unabsorbed light to the MS film layer for subsequent electron generation. Second, the NP underlayer can collect the light backscattered by the MS layer, efficiently enhancing the light harvesting. Additionally, the NP underlayer can also improve the connectivity with the FTO surface to improve the electron collection efficiency. $TiCl_4$ treatment is often used to improve the J_{sc}, V_{oc}, FF, and PCE of DSSCs. Although the effect mechanism is not clear yet, DSSCs after $TiCl_4$ treatment indeed have reduced recombination rate, prolonged electron lifetime, and improved electron collection efficiency. In this study, application of a DSL-18 underlayer and $TiCl_4$ post-treatment gives J_{sc} a significant increase to 18.02 mA cm^{-2} and consequently results in an enhanced PCE value to 10.32% (Figure 7a and Table 3). To attest the PCE results, we measured IPCE of the optimized DSSC (Figure 7b). The integrated current (16.99 mA cm^{-2}) of the IPCE spectrum matches the currents measured by $J-V$ within 5.7%. For comparison, we also prepared the DSL-18-based photoanode with the same thickness and assembled it to a DSSC under the same conditions. From Figure 7 and Table 3, we can see that the DSL-18 nanoparticle-based DSSC shows a much lower IPCE and PCE than the optimized TiO_2 MS-based DSSC.

Besides, the optimized TiO_2 MS-based DSSC shows a higher V_{oc} than the DSL-18-based DSSC, which can be evidenced by the dark current characterization. From Figure 7b, it can be seen that the DSL-18-based DSSC possesses a higher dark current at the same potential above 0.6 V, suggesting that the optimized DSL-18-based DSSC has a higher electron recombination rate than a TiO_2 MS-based DSSC. The higher recombination rate should be the reason for the lower V_{oc} value of the optimized DSL-18-based DSSC. EIS measurements under illumination were also conducted to investigate the recombination rate of the optimized DSL-18- and TiO_2 MS-based DSSCs. From Figure 8 and Table 4, we can see that after optimization by adding a DSL-18 nanoparticle layer and $TiCl_4$ treatment, the TiO_2 MS-based DSSC exhibits a larger recombination resistance and longer electron lifetime than the DSL-18-based DSSC. As a comparison and to illustrate the effect of the $TiCl_4$ treatment on the charge recombination rate and electron lifetime, we also measured the EIS data of both of the DSSCs without $TiCl_4$ treatment. As shown in Figure 8 and Table 4, without $TiCl_4$ treatment, the TiO_2 MS-based DSSC shows a slightly lower R_{ct} but a longer lifetime than the DSL-18-based DSSC, whereas after $TiCl_4$ treatment, the R_{ct} and τ_n values of the TiO_2 MS-based DSSC were all higher than that of the DSL-18-based DSSC. Also, the R_{ct} and τ_n values after $TiCl_4$ treatment were all higher than that of both of the DSSC without $TiCl_4$ treatment. These results suggest that $TiCl_4$

Table 3. Comparison of the Photovoltaic Properties Measured under 1 Sun Illumination for Optimized TiO_2 MS- and DSL-18-based DSSCs

cell	thickness (μm)	J_{sc} (mA cm^{-2})	V_{oc} (V)	FF (%)	η (%)
DSL-18+TiO_2 MS	4.8 + 7.6	18.02	0.772	74.2	10.32
DSL-18	12.5	13.83	0.749	73.6	7.63

DOI: 10.1021/acsami.5b02195
ACS Appl. Mater. Interfaces 2015, 7, 10928−10934

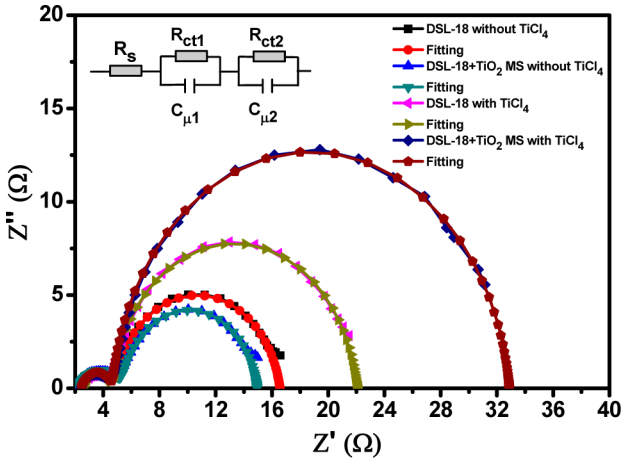

Figure 8. Nyquist plots of DSL-18+TiO_2 MS and DSL-18-based DSSCs with and without $TiCl_4$ treatment measured under 1 sun illumination.

Table 4. Electron Transfer and Recombination Resistance (R_{ct}) and Chemical Capacitance (C_μ) of the Optimized TiO_2 MS- and DSL-18-Based DSSCs with and without $TiCl_4$ Treatment Measured under 1 Sun Illumination

cell	$TiCl_4$ treatment	R_{ct} (Ω)	C_μ (μF)	$\tau_{n(EIS)}$ (ms)
DSL-18	N	11.7	141	16.5
DSL-18+TiO_2 MS	N	9.6	225	20.3
DSL-18	Y	17.4	147	25.6
DSL-18+TiO_2 MS	Y	28.2	127	35.8

treatment in DSSCs can indeed improve the charge recombination and that $TiCl_4$ treatment in TiO_2 MS-based DSSC has a more outstanding effect than in the nanoparticle-based DSSC.

3. CONCLUSIONS

TiO_2 microspheres were successfully synthesized via a solvothermal method in acetone. The TiO_2 microspheres were composed of densely interconnected crystals, exhibiting relatively high BET surface area, and were employed as a working photoanode for DSSC. Because of the higher dye-loading capacity and superior light-scattering effect, the microsphere-based DSSC gives a much higher J_{sc} and PCE value compared with the commercial DSL-18 paste. By optimizing the electrode employing a TiO_2 nanocrystal underlayer and $TiCl_4$ post-treatment, a high PCE of 10.32% was obtained. However, because of the small crystal size of the microspheres, the TiO_2 MS-based DSSC showed a much smaller recombination resistance, inducing a decrease of the electron collection efficiency. Thus, maximizing the crystal size while maintaining high BET surface area of such TiO_2 MS will be an important next step. We hope that the modified TiO_2-based DSSC will have a better performance than now, and the work is under way.

4. EXPERIMENTAL SECTION

Synthesis of TiO_2 Microspheres. All chemicals were used as received. Mesoporous TiO_2 microspheres were synthesized via a modified nonaqueous solvothermal process based on the previous reported method.[4] In a typical synthesis, titanium isopropoxide (TIP, 2 mL) was rapidly mixed with 50 mL of anhydrous acetone. The mixture was stirred for 10 min under ambient conditions and then transferred to a 100 mL Teflon-lined stainless-steel autoclave. After treatment at 200 °C for 12 h, the yellowish-brown precipitate was collected by centrifugation, washed with ethanol several times, and dried at 60 °C.

Assembly of Dye-Sensitized Solar Cells. For the photoanode, single-layer films of interconnected TiO_2 particles (either DSL-18 or TiO_2 MS) were screen-printed on FTO-type TCO glass through a 34T meshsize screen. The films were sintered at 510 °C for 30 min before solar cell construction. A 300 μM portion of cheno-3a,7a-dihydroxy-5b-cholic acid was dissolved with an equimolar amount of C101 complex in a mixture of *tert*-butanol and acetonitrile solvent (1:1 by volume). After being washed by acetonitrile and dried in air, the overnight-sensitized electrodes were sealed using a 25 μm thick Surlyn gasket and melted by heating with the Pt-modified TEC15 TCO counter-electrode. The latter was prepared by spreading out a drop of 5 mM H_2PtCl_6 isopropyl alcohol solution onto the counter-electrode before treating it at 450 °C for 30 min under air. A hole was introduced in the counter-electrode by sand-blasting, allowing the internal space between the two electrodes to be filled with volatile electrolyte using a vacuum backfilling system, and then was sealed with a thin glass sheet. The electrolyte was composed of 1 M DMII, 50 mM LiI, 30 mM I_2, 0.5 M *tert*-butylpyridine, and 0.1 M GuNCS in a solvent mixture of 85% acetonitrile with 15% valeronitrile by volume.

Prior to measurements, the cell was masked by a square black tape with a 5 × 5 mm^2 aperture.

Instruments. The morphology of the samples was investigated by scanning electron microscopy (FEI XL-30 SFEG coupled to a TLD) and transmission electron microscopy (TEM, JEM-200CX; JEOL). XRD patterns were recorded using a Bruker-AXS Microdiffractometer (model D5005) with Cu Kα radiation (λ = 1.5406 Å). The surface area, pore volume, and pore size were evaluated by using a micromeritics nitrogen adsorption/desorption apparatus (TriStar II 3020 V1.03, Micromeritics Instrument Corporation). Ultraviolet−visible (UV−vis) diffuse reflectance spectroscopy (DRS) and UV−vis absorption spectroscopy were performed using the UV−vis spectrophotometer (SOLID3700, Shimadzu Co. Ltd., Japan).

The J−V measurements were carried out on a Keithley model 2420 digital source meter controlled by Test point software under a xenon lamp (100 mW cm^{-2}). The IPCE values were confirmed as a function of wavelength from 300 to 800 nm (PV Measurements, Inc.) for DSSCs. EIS data were recorded by a computer-controlled potentiostat (Autolab 320, Metrohm, Switzer land) in a frequency range of 10 mHz to 1000 kHz applied in the dark. An electrochemical workstation (IM6e, Zahner, Germany) was conducted to measure the intensity of the modulated photocurrent/photovoltage spectroscopy (IMPS/IMVS) with light-emitting diodes (LED, λ = 610 nm) driven by Export (Zahner, Germany). Small amplitude is 10% or less than that of the dc component provided by the LED, and the frequency range was from 300 mHz to 3 kHz.

AUTHOR INFORMATION

Corresponding Authors

*E-mail: solarhu@sina.com. Phone: +86 55165593222.
*E-mail: sydai@ipp.cas.cn. Phone: +86 1061772268.

Notes

The authors declare no competing financial interest.

ACKNOWLEDGMENTS

This work was supported by the National Basic Research Program of China (no. 2011CBA00700), the China Postdoctoral Science Foundation (no. 2014M551825), and the National Natural Science Foundation of China (nos. 21173228 and 61204075).

REFERENCES

(1) Pan, J. H.; Wang, X. Z.; Huang, Q.; Shen, C.; Koh, Z. Y.; Wang, Q.; Engel, A.; Bahnemann, D. W. Large-scale Synthesis of Urchin-like

DOI: 10.1021/acsami.5b02195
ACS Appl. Mater. Interfaces 2015, 7, 10928−10934

Mesoporous TiO_2 Hollow Spheres by Targeted Etching and Their Photoelectrochemical Properties. *Adv. Funct. Mater.* **2014**, *24*, 95−104.
(2) Chen, Q.; Ren, B.; Zhao, Y.; Xu, X.; Ge, H.; Guan, R.; Zhao, J. Template-Free Synthesis of Core-Shell TiO_2 Microspheres Covered with High-Energy {116}-Facet-Exposed N-Doped Nanosheets and Enhanced Photocatalytic Activity under Visible Light. *Chem.—Eur. J.* **2014**, *20*, 17039−17046.
(3) Chen, X. B.; Liu, L.; Yu, P. Y.; Mao, S. S. Increasing Solar Absorption for Photocatalysis with Black Hydrogenated Titanium Dioxide Nanocrystals. *Science* **2011**, *331*, 746−750.
(4) Liu, B.; Liu, L. M.; Lang, X. F.; Wang, H. Y.; Lou, X. W.; Aydil, E. S. Doping high-surface-area mesoporous TiO_2 microspheres with carbonate for visible light hydrogen production. *Energy Environ. Sci.* **2014**, *7*, 2592−2597.
(5) Zhang, G.; Wu, H. B.; Song, T.; Paik, U.; Lou, X. W. TiO_2 Hollow Spheres Composed of Highly Crystalline Nanocrystals Exhibit Superior Lithium Storage Properties. *Angew. Chem., Int. Ed.* **2014**, *53*, 12590−12593.
(6) Wang, H. Y.; Chen, J. Z.; Hy, S.; Yu, L. H.; Xu, Z. C.; Liu, B. High-surface-area Mesoporous TiO_2 Microspheres via One-step Nanoparticle Self-assembly for Enhanced Lithium-ion Storage. *Nanoscale* **2014**, *6*, 14926−14931.
(7) Oregan, B.; Gratzel, M. A low-cost, high-efficiency solar-cell based on dye-sensitized colloidal TiO_2 films. *Nature* **1991**, *353*, 737−740.
(8) Yue, G.; Tan, F.; Li, F.; Chen, C.; Zhang, W.; Wu, J.; Li, Q. Enhanced Performance of Flexible Dye-Sensitized Solar Cell based on Nickel Sulfide/Polyaniline/Titanium Counter Electrode. *Electrochim. Acta* **2014**, *149*, 117−125.
(9) Yue, G.; Zhang, X.; Wang, L.; Tan, F.; Wu, J.; Jiang, Q.; Lin, J.; Huang, M.; Lan, Z. Highly Efficient and Stable Dye-sensitized Solar Cells Based on Nanographite/polypyrrole Counter Electrode. *Electrochim. Acta* **2014**, *129*, 229−236.
(10) Wu, J.; Xiao, Y.; Tang, Q.; Yue, G.; Lin, J.; Huang, M.; Huang, Y.; Fan, L.; Lan, Z.; Yin, S.; Sato, T. A Large-Area Light-Weight Dye-Sensitized Solar Cell based on All Titanium Substrates with an Efficiency of 6.69% Outdoors. *Adv. Mater.* **2012**, *24*, 1884−1888.
(11) Chen, H.; Kou, D.; Chang, Z.; Zhou, W.; Zhou, Z.; Wu, S. Effect of Crystallization of $Cu_2ZnSnS_xSe_{4-x}$ Counter Electrode on the Performance for Efficient Dye-Sensitized Solar Cells. *ACS Appl. Mater. Interfaces* **2014**, *6*, 20664−20669.
(12) Lee, S.-W.; Ahn, K.-S.; Zhu, K.; Neale, N. R.; Frank, A. J. Effects of $TiCl_4$ Treatment of Nanoporous TiO_2 Films on Morphology, Light Harvesting, and Charge-Carrier Dynamics in Dye-Sensitized Solar Cells. *J. Phys. Chem. C* **2012**, *116*, 21285−21290.
(13) Sauvage, F.; Chen, D.; Comte, P.; Huang, F.; Heiniger, L.-P.; Cheng, Y.-B.; Caruso, R. A.; Graetzel, M. Dye-Sensitized Solar Cells Employing a Single Film of Mesoporous TiO_2 Beads Achieve Power Conversion Efficiencies Over 10%. *ACS Nano* **2010**, *4*, 4420−4425.
(14) Chen, Y.; Huang, F.; Chen, D.; Cao, L.; Zhang, X. L.; Caruso, R. A.; Cheng, Y.-B. Effect of Mesoporous TiO_2 Bead Diameter in Working Electrodes on the Efficiency of Dye-Sensitized Solar Cells. *ChemSusChem* **2011**, *4*, 1498−1503.
(15) Docampo, P.; Guldin, S.; Steiner, U.; Snaith, H. J. Charge Transport Limitations in Self-Assembled TiO_2 Photoanodes for Dye-Sensitized Solar Cells. *J. Phys. Chem. Lett.* **2013**, *4*, 698−703.
(16) Cui, Y.; Zhang, L.; Lv, K.; Zhou, G.; Wang, Z.-S. Low Temperature Preparation of TiO_2 Nanoparticle Chains Without Hydrothermal Treatment for Highly Efficient Dye-sensitized Solar Cells. *J. Mater. Chem. A* **2015**, *3*, 4477−4483.
(17) Zhuge, F.; Qiu, J.; Li, X.; Gao, X.; Gan, X.; Yu, W. Toward Hierarchical TiO_2 Nanotube Arrays for Efficient Dye-Sensitized Solar Cells. *Adv. Mater.* **2011**, *23*, 1330−1334.
(18) Guo, M.; Yong, Z.; Xie, K.; Lin, J.; Wang, Y.; Huang, H. Enhanced Light Harvesting in Dye-Sensitized Solar Cells Coupled with Titania Nanotube Photonic Crystals: A Theoretical Study. *ACS Appl. Mater. Interfaces* **2013**, *5*, 13022−13028.
(19) Ding, Y.; Mo, L.-E.; Tao, L.; Ma, Y.-M.; Hu, L.-H.; Huang, Y.; Fang, X.-Q.; Yao, J.-X.; Xi, X.-W.; Dai, S.-Y. TiO_2 Nanocrystalline Layer as A Bridge Linking TiO_2 Sub-microspheres Layer and Substrates for High-efficiency Dye-sensitized Solar Cells. *J. Power Sources* **2014**, *272*, 1046−1052.
(20) Ding, Y.; Mo, L. e.; Tao, L.; Ma, Y.; Hu, L.; Jiang, L.; Li, Z.; Zhang, C.; Zhang, B.; Yao, J.; Dai, S. TiO_2 SUB-MICROSPHERES AS A BI-FUNCTIONAL SCATTERING LAYER FOR HIGH-PERFORMANCE DYE-SENSITIZED SOLAR CELLS. *Nano* **2014**, *9*, 1440007.
(21) Rui, Y.; Li, Y.; Zhang, Q.; Wang, H. Facile Synthesis of Rutile TiO_2 Nanorod Microspheres for Enhancing Light-harvesting of Dye-sensitized Solar Cells. *CrystEngComm* **2013**, *15*, 1651−1656.
(22) Shang, G.; Wu, J.; Huang, M.; Lan, Z.; Lin, J.; Liu, Q.; Zheng, M.; Huo, J.; Liu, L. Improving the Photovoltaic Performance of A Dye-sensitized Solar Cell by Using A Hierarchical Titania Bur-like Microspheres Double Layered Photoanode. *J. Mater. Chem. A* **2013**, *1*, 9869−9874.
(23) Hwang, S. H.; Yun, J.; Jang, J. Multi-Shell Porous TiO_2 Hollow Nanoparticles for Enhanced Light Harvesting in Dye-sensitized Solar Cells. *Adv. Funct. Mater.* **2014**, *24*, 7619−7626.
(24) Wu, W.-Q.; Xu, Y.-F.; Rao, H.-S.; Feng, H.-L.; Su, C.-Y.; Kuang, D.-B. Constructing 3D Branched Nanowire Coated Macroporous Metal Oxide Electrodes with Homogeneous or Heterogeneous Compositions for Efficient Solar Cells. *Angew. Chem., Int. Ed.* **2014**, *53*, 4816−4821.
(25) Lin, J.; Heo, Y.-U.; Nattestad, A.; Yamauchi, Y.; Dou, S. X.; Kim, J. H. Mesoporous Hierarchical Anatase for Dye-sensitized Solar Cells Achieving Over 10% Conversion Efficiency. *Electrochim. Acta* **2015**, *153*, 393−398.
(26) Lin, J.; Heo, Y.-U.; Nattestad, A.; Sun, Z.; Wang, L.; Kim, J. H.; Dou, S. X. 3D Hierarchical Rutile TiO_2 and Metal-free Organic Sensitizer Producing Dye-sensitized Solar Cells 8.6% Conversion Efficiency. *Sci. Rep.* **2014**, *4*, 1−8.
(27) Heiniger, L.-P.; Giordano, F.; Moehl, T.; Graetzel, M. Mesoporous TiO_2 Beads Offer Improved Mass Transport for Cobalt-Based Redox Couples Leading to High Efficiency Dye-Sensitized Solar Cells. *Adv. Energy Mater.* **2014**, *4*, 1400168.
(28) Huang, F.; Chen, D.; Zhang, X. L.; Caruso, R. A.; Cheng, Y.-B. Dual-Function Scattering Layer of Submicrometer-Sized Mesoporous TiO_2 Beads for High-Efficiency Dye-Sensitized Solar Cells. *Adv. Funct. Mater.* **2010**, *20*, 1301−1305.
(29) Garnweitner, G.; Antonietti, M.; Niederberger, M. Nonaqueous Synthesis of Crystalline Anatase Nanoparticles in Simple Ketones and Aldehydes As Oxygen-supplying Agents. *Chem. Commun.* **2005**, *3*, 397−399.
(30) Lei, B.-X.; Zhang, P.; Qiao, H.-K.; Zheng, X.-F.; Hu, Y.-S.; Huang, G.-L.; Sun, W.; Sun, Z.-F.; Zhang, X.-X. A facile template-free route for synthesis of anatase TiO_2 hollow spheres for dye-sensitized solar cells. *Electrochim. Acta* **2014**, *143*, 129−134.
(31) Nakade, S.; Matsuda, M.; Kambe, S.; Saito, Y.; Kitamura, T.; Sakata, T.; Wada, Y.; Mori, H.; Yanagida, S. Dependence of TiO_2 Nanoparticle Preparation Methods and Annealing Temperature on the Efficiency of Dye-Sensitized Solar Cells. *J. Phys. Chem. B* **2002**, *106*, 10004−10010.
(32) Nakade, S.; Saito, Y.; Kubo, W.; Kitamura, T.; Wada, Y.; Yanagida, S. Influence of TiO_2 Nanoparticle Size on Electron Diffusion and Recombination in Dye-Sensitized TiO_2 Solar Cells. *J. Phys. Chem. B* **2003**, *107*, 8607−8611.
(33) Wu, W.-Q.; Xu, Y.-F.; Rao, H.-S.; Su, C.-Y.; Kuang, D.-B. Trilayered Photoanode of TiO_2 Nanoparticles on a 1D-3D Nanostructured TiO_2-Grown Flexible Ti Substrate for High-Efficiency (9.1%) Dye-Sensitized Solar Cells with Unprecedentedly High Photocurrent Density. *J. Phys. Chem. C* **2014**, *118*, 16426−16432.

DOI: 10.1021/acsami.5b02195
ACS Appl. Mater. Interfaces 2015, 7, 10928−10934